SAND2012-2024C

Electrical and Thermal Finite Element Modeling of Arc Faults in Photovoltaic Bypass Diodes

Jay Johnson
Ward Bower
Michael Quintana
Sandia National Laboratories
P.O. Box 5800 MS0352
Albuquerque, NM 87185
e-mail: jjohns2@sandia.gov

ABSTRACT

Arc faults in photovoltaic (PV) modules have caused multiple rooftop fires. The arc generates a high-temperature plasma that ignites surrounding materials and subsequently spreads the fire to the building structure. While there are many possible locations in PV systems and PV modules where arcs could initiate, bypass diodes have been suspected of triggering arc faults in some modules. In order to understand the electrical and thermal phenomena associated with these events, a finite element model of a busbar and diode was created. Thermoelectrical simulations found Joule and internal diode heating from normal operation would not normally cause bypass diode or solder failures. However, if corrosion increased the contact resistance in the solder connection between the busbar and the diode leads, enough voltage potential would be established to arc across micron-scale electrode gaps. Lastly, an analytical arc radiation model based on observed data was employed to predicted polymer ignition times. The model predicted polymer materials in the adjacent area of the diode and junction box ignite in less than 0.1 seconds.

1. INTRODUCTION

Photovoltaic (PV) arc faults have led to a number of rooftop fires that have caused significant property damage and threatened the safety of building occupants [1-3]. Series arc faults in PV systems are the result of a discontinuity in the electrical path because of corrosion, diurnal thermal cycling, damage from rodents or weather, or other failure modes. Extensive failure analysis is undertaken to identify the failure modes in reported arc fault cases, but does not always identify the arc initiation site. The discontinuity can occur in connections in the array (e.g., fuses, connectors between modules, inverters, or combiner boxes) or within the module itself (e.g., junction boxes, bypass diodes, cell-to-cell collector ribbon connections, or collector ribbons-to-bus connections) [4-9]. Figure 1 shows modules before and after an arc has occurred in two different places. In one Sandia National Laboratories (SNL) study [10], a solder bond failed in a junction box, which caused the module to drop in and out of the string intermittently. This condition is a precursor to an arcing event, because the continuity of the electrical system is maintained by physical containment of the potting material in the junction box.

Within the module there are dozens of connections that can fail, shown in Figure 2. These connections should be designed to ensure (1) there is limited coefficient of thermal expansion (CTE) mismatch, (2) surrounding materials are fire-resistant, (3) there is an absence of galvanic reactions or other electrochemical corrosion, and (4) the manufacturing process is consistent. There is limited published work on thermal, electrical, and mechanical effects of arc faults within PV modules. Strauch et al. investigated the transient effects of arcing between a collector ribbon and busbar in a crystalline silicon (Si) module by first demonstrating that the ionization of air was possible with typical PV module voltages across a 5-micron gap, and then performing a thermomechanical analysis assuming a 5000 K plasma at the arcing location [11]. Because of the large number of failed bypass diodes in the field [12] and a relatively well-publicized junction box arc fault issue [13], the bypass diodes were selected for additional analysis.

As shown in Figure 3, the bypass diode is activated when the PV module is shaded because of the voltage mismatch with illuminated modules (details in References 14-16). An example diode is shown in Figure 4. It has been postulated that in installations where there is frequent shading, the bypass power diodes are regularly activated and are more

likely to cause arc fault fires [17]. Although the anecdotal evidence is inconclusive, high-temperature excursions due to Joule heating would accelerate failures in conducting bypass diodes. In this paper, the first study investigats the thermal behavior from Joule heating in the diode when there is no corrosion or gap in the electrical conductor. Results show a temperature increase from resistive heating less than 20 °C, so the diode heating does not significantly contribute to the degradation of the connection.

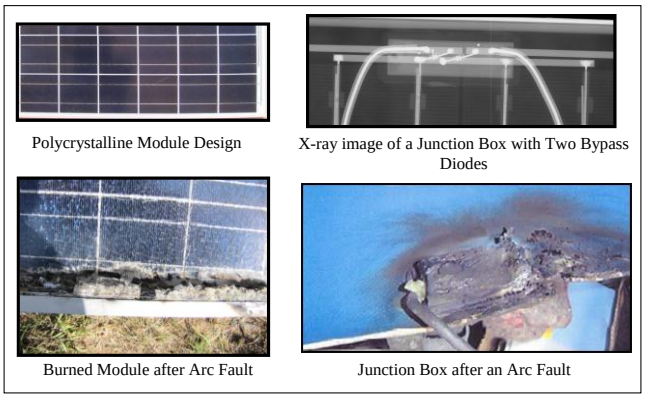

Fig. 1: Arc faults in two different PV modules.

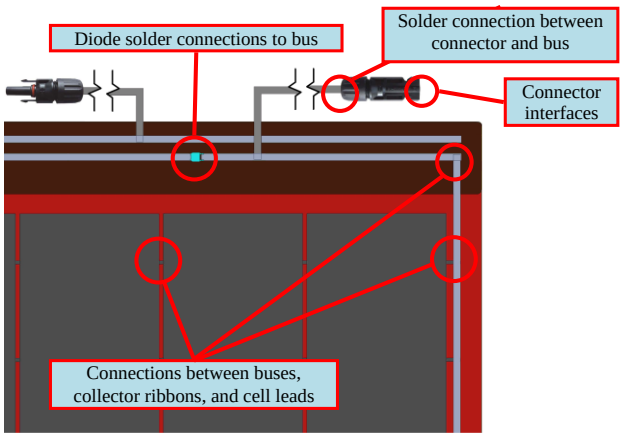

Fig. 2: Fictitious module design showing locations where there may be arc faults because of corrosion or conductor discontinuities.

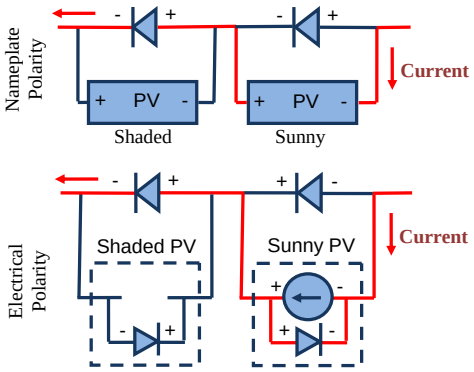

Fig. 3: PV bypass diode concept with nameplate and electrical polarities.

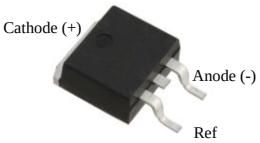

Fig. 4: Example solid-state 600-volt, 6-amp Si diode.

Since normal Joule heating would not cause diode failures alone, it was speculated that corrosion may also play a role in the cyclic heating and subsequent failure of the diode. To simulate diode corrosion, the contact resistance was increased at the diode solder connections to determine the change in voltage drop and temperatures. Finite element analysis (FEA) simulations showed that when the solder connection conductivity is reduced to 0.2% of the conductivity of solder, the voltage drop becomes large enough to arc across 1-µm gaps; and at 0.01% of the original conductivity, arcs can bridge 10-µm gaps. Lastly, assuming an arc has been initiated, polymers in the assembly were analyzed for ignition and burn-through times. Based on the proximity of the connection to the polymeric back sheet and estimated radiation power densities, the arc would ignite the back sheet in less than 0.1 sec.

2. ELECTRICAL AND THERMAL MODELING OF A BYPASS DIODE

A solid model of a bypass bus with a diode and the high-voltage output bus was created in SolidWorks. The external dimensions of the model are shown in Figure 5. This geometry was imported into COMSOL Multiphysics 4.1 for the arc fault simulations. The finite element mesh is shown in Figure 6.

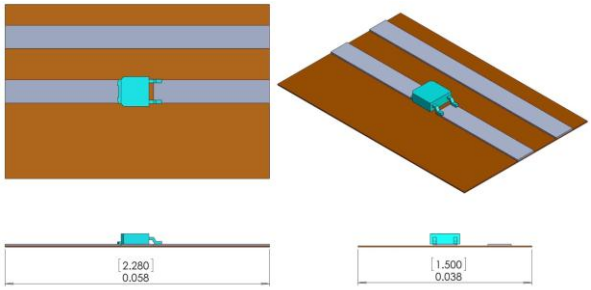

Fig. 5: Dimensions in the geometric model for the diode. Dual dimensions are in [inches] meters.

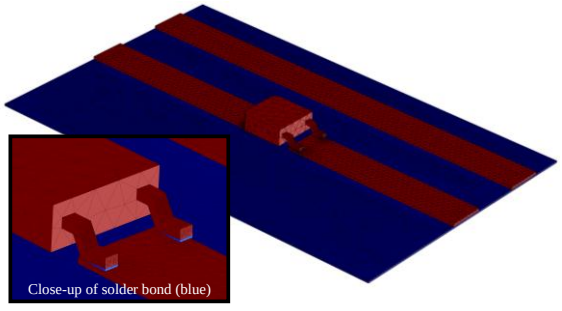

Fig. 6: Meshed diode model.

The buses and diode are modeled as 50/50 tin plating on copper, the back sheeting material is a generic thermoplastic, and the solder is assumed to be 60Sn-40Pb. The fidelity of the diode model could be greatly improved with information about the semiconductor and molding compound. The heating within the diode will be underpredicted in this model because the thermal conductivity of the package is lower than tin-plated copper; however, since this component is a commercial off-the-self microelectronics package, the diode is expected to survive the thermal loading and its internal temperature profile is not studied here. The associated material properties are shown in Table 1. The values for tin-plated copper busbar were determined as an average of tin and copper.

TABLE 1: ELECTRICAL AND THERMAL MATERIAL PROPERTIES USED IN THE MODEL

Material	Electrical Conductivity σ [S/m]	Relative Permittivity ε_r [-]	Thermal Conductivity k [W/m-K]
Thermoplastic	0.004	2.25	0.5
Sn-plated Cu	3.43×10^7	1.00	234
60Sn-40Pb Solder	6.67×10^6	1.00	50

Two electrical simulations were performed:
(1) The diode in forward bias with 5-amp current, representing a PV string with one shaded module. The goal of the simulation was to quantify the Joule and diode heating during normal operation and determine if this power dissipation could result in solder bond failures.
(2) The contact resistance between the solder and the bus was adjusted to represent different solder connection qualities (e.g., perfect conductivity, reduced conductivity from corrosion, open-air gap between the solder and the bus). By increasing the resistance, the voltage increased across the corroded region until arcing occurred. This study showed significant connection degradation is required to arc across a 5-micron gap.

In the simulations, the electrical behavior of the system is governed by the current conservation equation,

$$\nabla \cdot \mathbf{J} = 0, \tag{1}$$

where **J** is the current density in A/m^2 and the system is at steady state. Ohm's law is represented by

$$\mathbf{J} = \sigma \mathbf{E} + \mathbf{J}_{external}, \tag{2}$$

where σ is the electric conductivity of the materials, and $\mathbf{J}_{external}$ is the externally applied current density. The continuity equation for the electric potential is given by

$$\mathbf{E} = -\nabla \mathrm{v}, \tag{3}$$

where **E** is the electric field intensity in V/m, and v = v(x,y,z) is the electric potential at point (x,y,z). There is also a constitutive relation between the relative permittivity and the displacement current. The electric field for dielectric materials is described by

$$\mathbf{D} = \varepsilon_0 \varepsilon_r \mathbf{E}, \tag{4}$$

where **D** is the electric displacement field, ε_0 is the electric constant, and ε_r is the relative static permittivity of the material.

When the contact resistance is included in the model, the current at the boundary is described by

$$\mathbf{n} \cdot \mathbf{J}_1 = \frac{\sigma}{d}(\mathrm{v}_1 - \mathrm{v}_2) \tag{5}$$

$$\mathbf{n} \cdot \mathbf{J}_2 = \frac{\sigma}{d}(\mathrm{v}_2 - \mathrm{v}_1) \tag{6}$$

where *d* is the thickness of the layer, σ is the conductivity, indices 1 and 2 refer to the two sides of the boundary, and **n** is the normal vector.

The heating in the steady state case is calculated from the heat equation,

$$-k\nabla^2 T = Q_{joule} + Q_{diode}, \tag{7}$$

where $T = T(x,y,z)$ is the temperature field, *k* is the thermal conductivity of the material, and *Q* is the heat generation from power dissipation (i^2R losses) in W/m^3 due to Joule heating and forward-biased diode self-heating.

2.1 Diode in Normal Operation

In order to determine the diode heating during normal bypass operation, the current density to produce a total of 5 amps was generated at the end of the bypass bus. The current density boundary condition is given by

$$-\mathbf{n} \cdot \mathbf{J} = J_{bus}, \tag{8}$$

where J_{bus} is 5 amps divided by the cross-sectional area of the bus, or approximately 2.58×10^6 A/m^2. The current density boundary condition was selected because PV modules are current sources and the voltage drop across the entire bus was unknown. The generic module design has the connectors in this version attached at the center of the positive and negative buses, so the positive bus within the model subdomain is open and carries no current.

The bypass diode will produce heat under normal conducting operations. The power dissipated by the diode can be estimated by the product of the diode current and the turn-on

voltage of the diode. The turn-on voltage is nearly constant for all conducting currents so this value estimates the diode voltage drop well. The voltage drop depends on the bandgap of the semiconducting material and the current and voltage ratings of the diode. For high-power Si Schottky diodes on the market, the turn-on voltage is often between 0.4 and 0.5 volts [16]. Here we assume the diode voltage drop is 0.45 volts. Since the current through this module is 5 amps, the forward-biased self-heating power dissipated by the diode is 2.25 watts. This dissipative power is modeled by a power source uniformly generating heat within the diode volume.

As shown in the results of the simulation in Figure 7, there were low resistive losses from the bus and diode materials, and the voltage drop through the model excluding the diode voltage drop was 4.3 mV. The high-voltage output bus has low electrical resistance, so the voltage was maintained at a uniform 2.15 mV. The current density was uniform along the bypass bus, but once it reached the diode leads it increased to 1.1×10^7 A/m^2, as shown in Figure 8. Furthermore, as illustrated by the vector field traces and surface current vector field in Figure 8 and Figure 9, the current is concentrated through the gull-wing leads, which results in higher Joule heating in those regions.

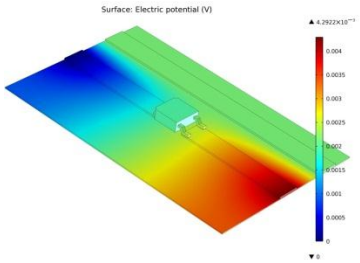

Fig. 7: Electric potential, excluding 0.45 V diode voltage drop, in the diode subdomain with 5 amps passing through the bus.

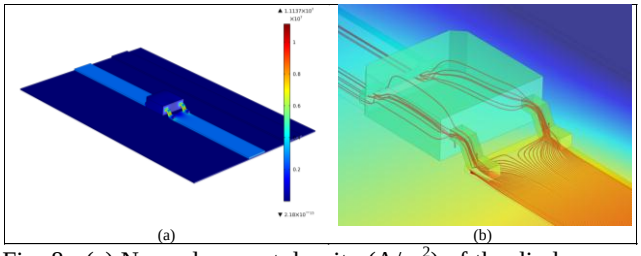

Fig. 8: (a) Normal current density (A/m^2) of the diode model and (b) electron traces through the diode.

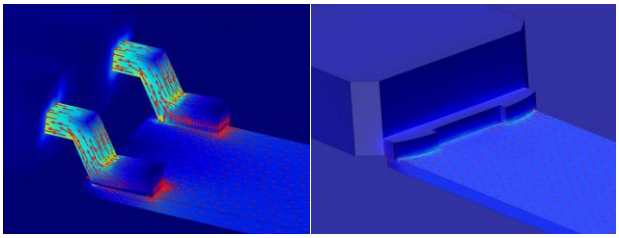

Fig. 9: The current vector field in the diode leads. The greatest current density is in the gull-wing leads.

2.2 Joule and Diode Heating

The exterior polymer walls and busbar end faces were set to 20 °C to calculate the steady state temperature of the diode and bypass busbar during forward biasing. Convective and radiative heat transfer were not included because the diode was assumed to be in a junction box or other enclosure. The diode heated to 0.32 ºC above ambient with resistive power dissipation alone, but the diode internal heating from the semiconductor voltage drop increased the diode temperature an additional 68.05 ºC above ambient, as shown in Figure 10. Thus, the diode heating from the forward-biased voltage drop in the semiconductor accounted for the 99.5% of the heating. The thermal increase is consistent with field measurements showing diodes in junction boxes reaching as much as 150 to 200 ºC during shading events in the field [15], where ambient is often 30-40 ºC and the difference in module temperature and ambient can reach 40 ºC or larger [18].

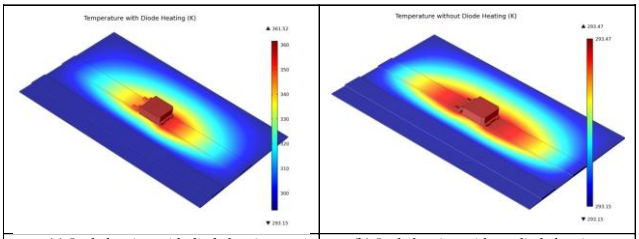

(a) Joule heating with diode heating Diode temperature: 88.37 ºC

(b) Joule heating without diode heating Diode temperature: 20.32 ºC

Fig. 10: Steady state temperature profile of the diode model (a) with and (b) without diode heating.

In order to determine the rate of heating in the diode, a transient study was performed with material properties shown in Table 2. Equation (7) was replaced with the transient equation,

$$\rho C_p \frac{\partial T}{\partial t} - k\nabla^2 T = Q\,, \qquad (9)$$

where the transient heating rate of the system is determined by the density, ρ, and heat capacity, C_p, of the materials [19].

TABLE 2: TRANSIENT MODEL MATERIAL PROPERTIES.

Material	**Density ρ [kg/m^3]**	**Heat Capacity C$_p$ [J/kg-K]**
Thermoplastic	1160	2300
Sn plated Cu	8030	306
60Sn-40Pb Solder	9000	150

The simulation demonstrated the time scales for diode and busbar heating when a shadow caused the bypass diode to conduct. Snapshots of the transient heating simulation are shown in Figure 11. The solution asymptotically approaches steady state solution in approximately 1 minute, shown in Figure 12. This simulation provides a reference case for "normal" or "baseline' thermal heating in the diode.

Since the diode temperature change was 68.37 °C when

activated, it is possible, but unlikely, there could be thermal management issues in modules that regularly use bypass diodes. Power diodes are typically rated to temperatures of 150 ºC and above. Further, the melting temperature of 60Sn-40Pb solder is 183 ºC (456.2 K), so under normal operation the diode will be well below the melting point, although cyclic thermal loading could cause bond failures. Soldered parts often are fatigue tested with 10 to 1000 thermal cycles between -55 and 150 °C to meet Military Specifications [20] or JEDEC Standards [21]. However, there is no accelerated life testing for PV bypass diodes in international module qualification testing. IEC 61215-10.18 [22] requires the diode operate at 75 ºC at both 1.00 and 1.25 times the short circuit current for 1 hour. In the field, thermal fatigue can cause the bypass diodes to fail when the diodes conduct frequently because of cloudy conditions or diurnal shading from a tree, chimney, or other structure. One common failure mode from thermal fatigue is the CTE mismatch between diode and junction box components, which leads to separation in solder joints or wire bonds. In that case, the conductor gap can then produce a series arc fault.

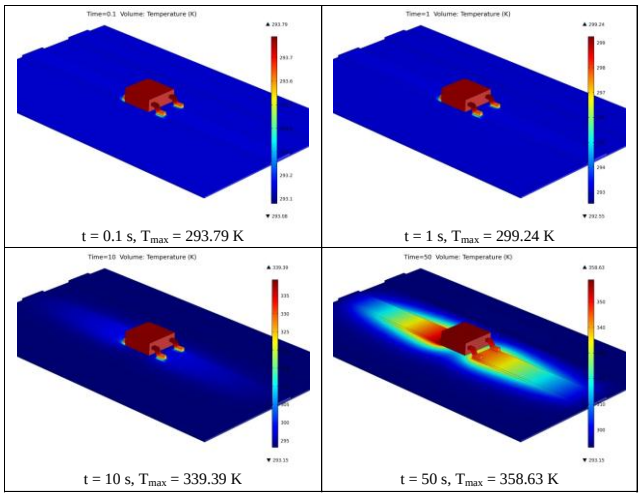

Fig. 11: Temperature distribution from Joule and internal heating of the diode for different simulation times.

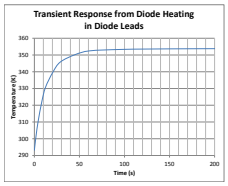

Fig. 12: Transient diode thermal model reaching steady state with thermal measurements taken at diode leads.

2.3 Diode Degradation

In order to simulate corrosion and electrical degradation of the diode, contact resistance was added to the model between the bus and the diode, shown in Figure 13. In the previous section, there was a low voltage drop (4.3 mV) through the diode when the bypass diode was conducting properly. This voltage drop increases as the solder bond degrades because the electrical conductivity of 60Sn-40Pb solder is 6.5×10^3 S/m but the electrical conductivity of air is ~5.5×10^{-15} S/m [23]. This analysis investigated the thermoelectrical behavior of the diode subdomain for conductivities between that of a good solder bond to an open connection, though, even without a catastrophic solder failure, thermal cycling can decrease the thermal conductivity of the soldered joints [24].

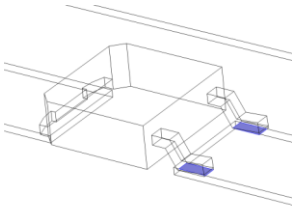

Fig. 13: Location of contact resistance from corrosion.

A parametric study was performed taking the conductivity of the contact resistance from air (5.5×10^{-15} S/m) to solder (6.5×10^3 S/m) and up to Cu/Sn (3.5×10^7 S/m) using Equations (5) and (6). The results are shown in Figure 14 for an assumed gap distance d = 5 μm. There is a low voltage drop from σ = 10 to 1×10^7 S/m, but the voltage drop increases to 7.16 volts at 1 S/m. This is less than 0.02% of the electrical conductivity of solder so there would be significant degradation of the solder joint to achieve this voltage across the gap. The dielectric strength of air is 3000 V/mm or 3 V/μm [25, 26] at standard temperature and pressure (STP). When a gap size, *d*, has a potential $v = |v_1 - v_2| = 3$ V/μm across it, air will ionize and form an arc. Therefore, based on the voltage across the gap, the minimum safe (non-arcing) gap in microns is

$$d = \frac{v}{3\,\mathrm{V}/\mu\mathrm{m}}, \qquad (10)$$

although, in the case of the actual diode, the gap will not contain pure air, but rather a combination of outgassed organics (e.g., hydrocarbons from adhesives) and, in some modules, encapsulant material inside the junction box. These materials and gasses will have different dielectric strengths, and therefore will not arc at the same gap potential.

The plot of gap voltages in Figure 14 contains horizontal lines representing the minimum voltages required to arc across different size air gaps. Smaller gaps of 1 and 2 microns will experience arcing when the electrical conductivity decreases from 10 and 1 S/m, and once the conductivity degrades to 0.1 S/m, gaps of 20 μm will begin arcing. The large potential increase at approximately $\sigma = 1 \times 10^{-5}$ S/m is attributed to the increased diode resistance and the current path shifting to the back sheet, shown in Figure 15. Note that most PV strings would not be able to supply more than 600 volts, so the current density boundary conditions are not valid below 0.01 S/m. Therefore, using Equation (10), the maximum gap that could initiate an arc in a 600-volt system is 0.2 mm.

Unfortunately, it is difficult to know what level of degradation is required to reduce the electrical conductivity of the diode solder to these values. In connectors with different materials,

galvanic corrosion could steadily degrade the connection until there was a gap and enough potential to cause an arc. In the case of the soldered diode, a crack failure due to thermal fatigue or joint stress is more likely. If the diode connection was loose it is possible that the electrical conductivity of the joint would rapidly diminish. It should also be noted that if there was a thin metal connection (analogous to a fuse) between the solder and the Sn/Cu bus, significantly less voltage would trigger the arc because the current would burn through the connection and generate the arc. (This is the technique used with the arc fault generator in 1699B testing [27].) However, once the arc is triggered, the voltage across a burning arc drops significantly (1.2 to 1.3 V/mm [28-29]) because the resistance drops once the air is ionized and a high-temperature plasma is established [11].

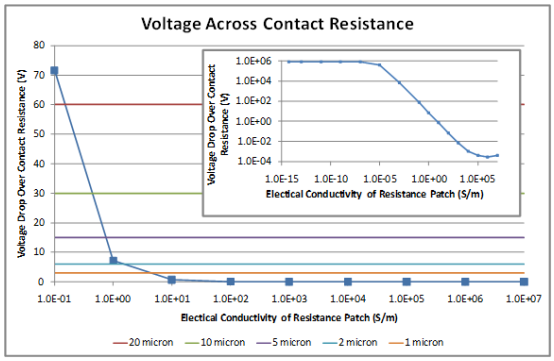

Fig. 14: The voltage drop over the solder connection with a 5-amp bus current. Horizontal lines show the threshold where arcing will begin to occur in air for different gap sizes.

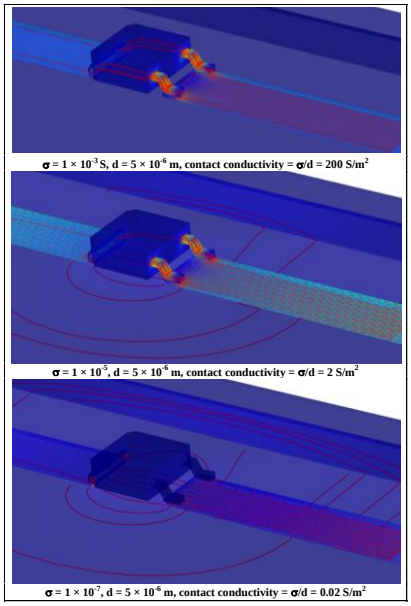

Fig. 15: Transition from diode acting as a conducting path to the plastic back sheet.

If an arc did not form from the large voltage gap, the temperature profile would closely match the voltage drop profile. The diode temperatures with electrical conductivities below 1 S/m increase significantly because of i^2R losses, shown in Figure 16. The σ/d term in Equations (5) and (6) defines the electrical conductivity between the bus and diode, and since the electrical conductivity is the reciprocal of electrical resistance (1/S = Ω), the electrical resistance and, hence, Joule heating, are linearly dependent on d and 1/σ.

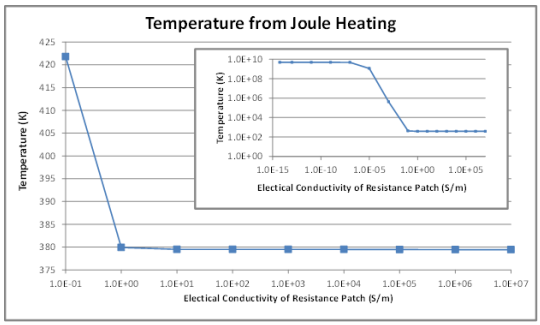

Fig. 16: The steady state temperature of the diode due to increasing ohmic losses.

3. PHYSICS OF ARCING

As shown above, sufficient degradation of the solder connections in PV systems will cause an arc to initiate. The arc is a plasma column between two electrodes of opposite polarity, established when the dielectric strength of the atmosphere is exceeded. While initially the atmosphere is an excellent insulator, the ionized plasma is an excellent conductor and the voltage drop across the gap decreases from 3000 V/mm to 1.2 V/mm. A diagram of the voltage drop across the arc gap is shown in Figure 17. With the arc established, the anode and cathode drop is relatively consistent for different electrode materials. Generally this voltage drop is 20 to 40 volts (for example, it is 23.5 V for copper, 26.5 V for steel, and 36 V for tungsten [30-31]).

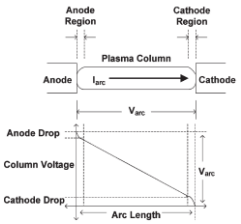

Fig. 17: Voltage characteristics of an arc across a gap [30,31].

The initiation and sustainment of the arc is dependent on a number of material and geometric considerations. Stokes and Oppenlander report, "the minimum voltage needed to maintain an arc depends on current magnitude, gap width, and orientation of the electrodes" [32]. Direct current (DC) arcs do not pass through zero current every half cycle like alternating current (AC) arcs so they are much more difficult to extinguish. However, the arc can be extinguished with arc-suppressing atmospheric conditions or an increasing gap distance. Unfortunately, PV arc faults often start in coated wiring, or around organic-based adhesives and epoxies. When exposed to the high temperatures of the arc plasma, these

materials pyrolyze and release combustible hydrocarbons that subsequently start PV fires [27]. With fire-retardant materials [33] the fire risk can be reduced. Hastings found that DC arcs will self-extinguish when the atmospheric conditions include flame-retardant chemistries [34]. The second option for self-extinguishing an arc is by burning the electrodes apart from each other. The arc resistance is linearly proportional to the arc gap for a given arc current [32], so as the gap widens, the resistance of the arc grows and eventually breaks the plasma column.

3.1 Polymer Burn Times

One of the biggest hazards from PV arc faults is igniting a fire in the PV materials which can spread to the building. The 5000 to 7000 K arc will melt metals and quickly vaporize and burn polymers that are in direct contact with the arc. However, the arc will also ignite materials that are separated from the plasma itself through radiative heating. It is difficult to estimate the time required to burn distanced PV materials, but some researchers have developed analytical relationships between arc wattage and burn times. In Figure 18, Hastings extrapolated surface ignition times from References 35 and 36 and estimated burn-through times based on arc radiation power densities. Hastings also determined an equation for burn-through times versus power density, although empirical results varied because of the chaotic nature of arcs [34].

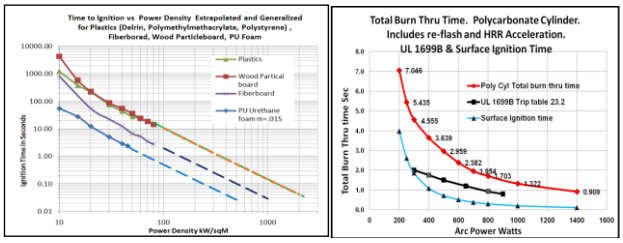

Fig. 18: Time to surface ignition versus power density and burn-through times for different arc powers when the arc is encapsulated by the polymer sheath [34].

The power density from Joule heating is not the same as the incident arc radiation on the materials, so the power density cannot be taken directly from the simulation. To estimate the power in the PV arc, the string voltage change during an experimental arc is multiplied by the string current. Experimentation at SNL showed that a single string operating at 4 amps experienced roughly a 25-volt drop in string voltage during an arc [37]. Therefore, based on the conservation of energy, it is expected that 100 watts of radiation was generated by the arc. (This is one-third the power required for the arc tests in UL 1699B [38], but nearly five times the arc power of some arc fault circuit interrupter (AFCI) tests [39].) Assuming the arc is initiated at the interface between the diode lead and busbar, there is a small gap between the arc and the plastic back sheet. The area directly below the arc will be exposed to the greatest amount of radiation, so a representative patch is used to calculate the incident radiation. To calculate the view factor, the arc is modeled as a semi-infinite horizontal cylinder and the patch has infinite depth, shown on the right of Figure 19. The view factor from area A_1 to area A_2 is [40]

$$F_{1-2} = \frac{1}{\pi}\left[\tan^{-1}\left(\frac{w/2}{h}\right)\right]. \qquad (11)$$

The view factor is 0.041 for this geometry, meaning that 4.1% of the radiation produced by the arc will be incident on the 1-mm subdomain of the back sheet directly below the arc. Thus, the square (1 mm^2) region below the arc will experience approximately 4.1 watts of arc radiation, or 4100 kW/m^2. Based on this power density and extrapolating the data on the left side of Figure 18, the back sheet would ignite in less than 0.1 second. As the height decreases and the width increases, the view factor and incident radiation increase, as shown in Figure 20. As expected, if the arc was generated farther away from the plastic material it would take more time to combust. However, if the diode was potted, the radiation view factor for the encapsulant would be 1.0 because all the radiation energy would be absorbed by the surrounding material and ignite in less time. Thus, regardless of the geometry, materials in the vicinity of the arc fault will burn or melt in extremely short time periods.

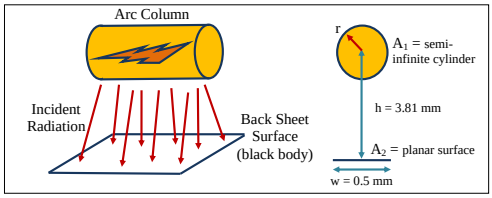

Fig. 19: Radiation model and view factor parameters.

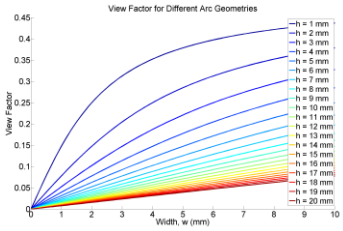

Fig. 20: View factors for different values of w and h, given that $r \leq h$.

4. CONCLUSIONS

Arc faults in rooftop PV systems have caused residential and commercial building fires. Due to the 2011 *National Electrical Code* ® standard requiring arc fault detection [41], there has been an expanded effort to understand the root cause and behavior of series arcs in PV systems. Series arcs result from the current bridging a conduction discontinuity in the electrical system. The discontinuity can form in modules, inverters, connectors, disconnects, or other connections. This study selected a bypass diode as a potential area for arcing because bypass diodes have been known to fail and there are documented cases of arcing in junction boxes.

To determine if frequent use of the bypass diode could lead to premature failure, the Joule and internal forward-bias heating

in a diode was studied with a finite element model in COMSOL. The study determined that there is a 68.37 °C temperature increase from diode operation in approximately 1 minute—but not enough to cause accelerated failures in diodes under normal operating conditions occurring from shading of modules. Next, corrosion was simulated at the diode solder connection to determine the correlation between contact resistance, gap voltage drop, and Joule heating. The arc will only jump the gap if there is enough electrical potential to cause the dielectric breakdown of the atmosphere between the electrodes. It was determined that for an air atmosphere, the resistance of the solder bond would have to increase 1000 times to create an arc across a 1-μm gap. However, once the arc is formed, the high-temperature plasma irradiates the surrounding material, igniting polymers and melting metals. A calculation using empirical measurements found that the polymeric back sheet would ignite in less than 0.1 sec.

This simulation studied the electrical and thermal behavior of one connection in a PV module. Additional simulations and experimental tests are needed to fully characterize the arc fault dangers in PV systems and identify how these hazards can be ameliorated or eliminated. Further, experimental validation is required to corroborate these simulations.

5. ACKNOWLEDGEMENTS

Sandia National Laboratories is a multi-program laboratory managed and operated by Sandia Corporation, a wholly owned subsidiary of Lockheed Martin Corporation, for the U.S. Department of Energy's National Nuclear Security Administration under contract DE-AC04-94AL85000. This work was funded by the US Department of Energy Solar Energy Technologies Program.

6. REFERENCES

(1) H. Haeberlin, Arc detector as an external accessory device for PV inverters for remote detection of dangerous arcs on the DC side of PV plants, EU PVSEC, Valencia, Spain 2010 (2) L. Ji, PV Fire: Experience and Studies, International Photovoltaic Reliability Workshop II, Tempe, AZ, July 31, 2009 (3) P. Jackson, Target Roof PV Fire of 4-5-09, City of Bakersfield, California, April 29, 2009 (4) J. Johnson, Overview of arc-faults and detection challenges, Solar ABCs, Feb. 8, 2010 (5) S. Kurtz, J. Granata, and M. Quintana, Photovoltaic-Reliability R&D toward a solar-powered world, SPIE Solar Energy & Technology Conference, San Diego, CA, Aug. 2-6, 2009 (6) A.M. Ricaud, R.C. Petersen, Environmental stress tests: acceleration of corrosion, 8th EU PV Solar Energy Conference, Florence, 1988, pp. 549-553 (7) T.J. McMahon and G.J. Jorgensen, Adhesion and thin-film module reliability, 4th World Conference on PV Energy Conversion, Waikoloa, HI, USA, 2006, pp. 2062-2065 (8) G.J. Jorgensen, et al., Moisture transport, adhesion, and corrosion protection of PV module packaging materials, Solar Energy Materials & Solar Cells, Vol. 90, pp. 2739-2775, 2006 (9) C. Whitaker, PG&E's perspectives on module reliability, NREL Photovoltaic Performance and Reliability Workshop (10) J. Johnson, et al., Characterizing PV arcing conditions with impedance spectroscopy and frequency response analysis, 26th EU PVSEC, Hamburg, 2011 (11) J. Strauch, et. al, PV module arc fault modeling and analysis, PV MRW, Golden, CO, Feb. 2011 (12) G. TamizhMani, et. al, Failure analysis of design qualification testing: 2007 VS. 2005, 33rd IEEE PVSC, May 11-16, 2008 (13) A. Schlumberger, A. Kreutzmann, Brennendes Problem – Schadhafte BP-Module können Feuer entfachen, Photon, Aug. 2006, pp. 104-106 (14) J.W. Bishop, Solar Cells, Vol. 25, pp. 73-89, 1988 (15) S.A. Fahrenbruch, Solar bypass diodes: then and now, Solar, Vol. VI, pp. 21-26, 2010 (16) D. Roche, H. Outhred, and R. John Kaye, Analysis and control of mismatch power loss in photovoltaic arrays, Prog. in Photovoltaics: Research and Applications, Vol. 3, pp. 115-127, 1995 (17) T. Zgonena, L. Ji, and D. Dini, Photovoltaic DC arc-fault circuit protection and UL Subject 1699B, PV MRW, Golden, CO, Feb. 2011 (18) M.C. Alonso García, J.L. Balenzategui, Renewable Energy, Vol. 29, No. 12, Oct. 2004, pp. 1997-2010. (19) F.P. Incropera, D.P. DeWitt, Introduction to Heat Transfer, 4th Ed., John Wiley & Sons, New York, 2002 (20) MIL-STD-883G, Test Method 1010, US DOD, 2006 (21) JEDEC Standard JESD22-A104, Temperature Cycling, 2005 (22) IEC 61215, 2nd Ed., 2005. (23) S.D. Pawar, P. Murugavel, and D.M. Lal, J. Geophysical Research, Vol. 114, D02205, 2009 (24) F. Guo, J.G. Lee, T. Hogan, and K.N. Subramanian, J. Materials Research, Vol. 20, No. 2, pp. 364-374, 2005 (25) P.A. Tipler, College Physics, Worth, p. 467, 1987 (26) J.S. Rigden, Macmillan Encyclopedia of Physics, Simon & Schuster, pp. 353, 1996 (27) D. Dini, P. Brazis, and K.-H. Yen, Development of arc-fault circuit-interrupter requirements for photovoltaic systems, 37th PVSC, Seattle, WA, June 19-24, 2011 (28) T.E. Browne, J. Electrochem. Soc., Vol. 102, No. 27, 1955.(29) A.P. Strom, Long 60-cycle arcs in air, Trans. Amer. Inst. Elect. Eng., Vol. 65, pp. 113-117, 1946. (30) V.P. Ignatko, 3rd Int. Symp. Switching Arc Phenom., pp. 98-102, 1977 (31) R.F. Ammerman, T. Gammon, P.K. Sen, and J.P. Nelson, IEEE Transactions on Industry Applications, Vol. 46, No. 5, pp.1810-1819, 2010 (32) A.D. Stokes and W.T. Oppenlander, J. Phys. D, Appl. Phys., Vol. 24, No. 1, pp. 26-35, Jan. 1991 (33) A.B. Morgan and M. Bundy, Cone calorimeter analysis of UL-94 V-rated plastics, Fire and Materials, Vol. 31, pp. 257-283, 2007 (34) J.K. Hastings, et al., A study of ignition time for materials exposed to dc arcing in PV systems, 37th PVSC, Seattle, WA, June 19-24, 2011 (35) V. Babrauskas, Ignition Handbook, Fire Science Publishers, 2003 (36) V. Babrauskas, and I. Wetterland, Comparative data from LIFT and cone calorimeter tests on 6 products, including flame flux measure-ments, SP Report 1999:14, Swedish National Testing and Research Institute, Borås (37) J. Johnson, et. al, Photovoltaic DC arc fault detector testing at Sandia National Laboratories, 37th PVSC, Seattle, WA, June 19-24, 2011. (38) Underwriters Laboratories Subject 1699B, Outline of investigation for photovoltaic DC arc-fault circuit protection, Apr. 29, 2011. (39) C.J. Luebke, et al., Field test results of DC arc fault detection on residential and utility scale PV arrays, 37th PVSC, Seattle, WA, June 19-24, 2011 (40) M.F. Modest, Radiative heat transfer, 2nd Ed., Academic Press, San Diego, CA, 2003 (41) National Electrical Code, 2011 Ed., NFPA70, National Fire Protection Association, Quincy, MA.